Polymer Chemistry

PAPER

View Article Online
View Journal | View Issue

Cite this: *Polym. Chem.*, 2018, **9**, 3684

Using benzoxazine chemistry and bio-based triblock copolymer to prepare functional porous polypeptide capable of efficient dye adsorption†

Cheng-Chang Tsai,[a] Zhihua Gan[b] and Shiao-Wei Kuo *[a,c]

Received 1st May 2018,
Accepted 15th June 2018

DOI: 10.1039/c8py00664d

rsc.li/polymers

A new biocompatible poly(ε-caprolactone-*b*-ethylene oxide-*b*-tyrosine) triblock copolymer (PCL-*b*-PEO-*b*-PTyr) has been synthesized through ring opening polymerization (ROP) employing PCL-*b*-PEO-NH_2 as a macro-initiator. The phenolic OH groups on the side chains of the PTyr block were subjected to Mannich condensations with CH_2O and aniline to form benzoxazine (BZ) units, which underwent thermal ROP to give the triblock copolymer PCL-*b*-PEO-*b*-PTyrBZ. This thermal crosslinking process formed a three-dimensional network structure, featuring a functional porous PTyr structure with phenolic OH and amide units, that enhanced the thermal stability of the triblock copolymer and allowed selective thermal cancelation of the PCL-*b*-PEO block segment. This functional porous PTyr displayed high adsorption capacity toward methylene blue (MB) in an aqueous solution, the result of hydrogen bonding between the nitrogen atom in the aromatic ring of MB and the phenolic OH or amide groups of the porous PTyr structure.

Introduction

Biopolymers (*e.g.*, polypeptides) are being use in many applications because of their biocompatibility, environmental friendliness, biodegradability, and flexible structural diversity.[1–5] The secondary structures of polypeptides, including α-helices and β-sheets stabilized through intra- and intermolecular hydrogen bonds, have been exploited for tissue engineering and the adsorbing of pollutants.[6–15] In a previous study, we incorporated polytyrosine (PTyr) within a mesoporous silica co-templated by the biodegradable diblock copolymer poly(ε-caprolactone-*b*-ethylene oxide) (PCL-*b*-PEO) and the PTyr homopolymer; selective solvent treatment removed the PCL-*b*-PEO diblock copolymer, leaving PTyr within the mesoporous silica and capable of dye absorption.[16] In this present study, we prepared a porous PTyr structure directly, also templated by a PCL-*b*-PEO diblock copolymer, but without the mesoporous silica.

Porous polypeptides are usually prepared using a polymer blend method, templated by another biodegradable polymer that is then selectively removed to form the porous structure.[17,18] Recently, various block copolymers—including PCL-*b*-PEO,[19–22] poly(ethylene oxide-*b*-styrene),[23,24] and poly(styrene-*b*-4-vinylpyridine)[25–27]—have been used as templates to prepare mesoporous phenolic resin or silica materials having high surface areas and pore volumes that are suitable for application in separation, adsorption, and drug delivery.[28–30] Although the polypeptide PTyr possesses phenolic OH units on its side chains, it is difficult to prepare porous PTyr structures when using diblock copolymers as templates. For example, PTyr/PEO and PTyr/PCL blends undergo macrophase separation because PTyr-favors strong intramolecular hydrogen bonding (to form the α-helix conformation) over inter-association hydrogen bonding of its phenolic OH groups with the ether units of PEO or the C=O groups of PCL.[31] Although the phenolic OH groups of PTyr can strongly interassociate though hydrogen bonds with the pyridyl groups of P4VP to form miscible blends,[32–34] it has been difficult to obtain porous structures from these blends because the thermal degradation of pure PTyr occurs at a lower temperature than that of P4VP.

To overcome the miscibility problems of PTyr/PEO and PTyr/PCL blends, here we synthesized a new biocompatible PCL-*b*-PEO-*b*-PTyr triblock copolymer [Scheme 1(b)] through ring opening polymerization (ROP) using amino-terminated PCL-*b*-PEO as the macro-initiator [Scheme 1(a)]. We took

[a]*Department of Materials and Optoelectronic Science, National Sun Yat-Sen University, Kaohsiung 80424, Taiwan. E-mail: kuosw@faculty.nsysu.edu.tw*
[b]*State Key Laboratory of Organic-Inorganic Composites, College of Life Science and Technology, Beijing University of Chemical Technology, Beijing 100029, China*
[c]*Department of Medicinal and Applied Chemistry, Kaohsiung Medical University, Kaohsiung, Taiwan*

†Electronic supplementary information (ESI) available: Chemical structures for FTIR and GPC spectra for monomers and polymers are shown in Fig. S1–S3. See DOI: 10.1039/c8py00664d

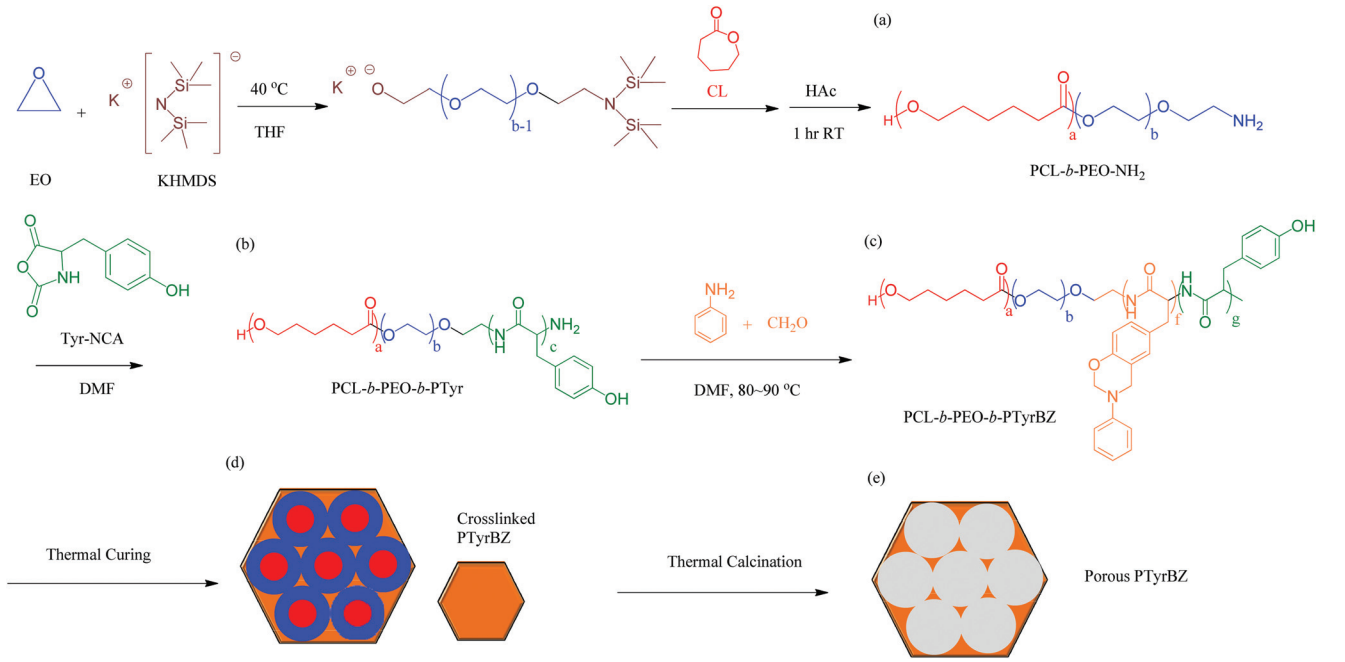

Scheme 1 (a–c) Preparation of (a) PCL-*b*-PEO-NH_2, (b) PCL-*b*-PEO-*b*-PTyr, and (c) PCL-*b*-PEO-*b*-PTyrBZ. (d) Microphase separation of the PCL-*b*-PEO-*b*-PTyrBZ triblock copolymer after thermal polymerization. (e) Functional porous PTyr obtained after thermal cancelation of the PCL-*b*-PEO block segment.

advantage of the phenolic OH groups on the side chains of PTyr to form benzoxazine (BZ) units, through Mannich condensation with paraformaldehyde and aniline [Scheme 1(c)], and then performed thermal ROP of the BZ units to increase the thermal stability of the triblock copolymer. This thermal crosslinking process resulted in a three-dimensional (3D) network structure of thermoset polybenzoxazine without the release of any byproducts. Generally, 3D network structures have many attractive applications because of their high thermal stability, low surface free energy, excellent mechanical properties, and dimensional stabilities.[35–40] Ultimately, we prepared a porous PTyr [Scheme 1(e)] through selected thermal cancelation of the PCL and PEO block segments after thermal crosslinking of PCL-*b*-PEO-*b*-PTyrBZ [Scheme 1(d)]. The chemical structures, thermal stability, thermal curing behavior, porous structures, and dye adsorption behavior of PCL-*b*-PEO-*b*-PTyrBZ and the resulting porous PTyr structures are discussed below.

Experimental section

Materials

Ethylene oxide (EO, BDH Limited Poole, England) was purified and dried over calcium hydride at 0 °C and stored at −20 °C prior to use. ε-Caprolactone (CL, Acros Organics) was dried over calcium hydride and purified through vacuum distillation at 70 °C prior to use. L-Tyrosine (MP Biomedicals), potassium bis(trimethylsilyl)amide (Alfa Aesar), triphosgene (TCI), butylamine (Sigma-Aldrich), aniline (Sigma-Aldrich), paraformaldehyde (Acros), and methylene blue hydrate (MB, Sigma-Aldrich) were purchased commercially. Acetonitrile (MeCN, Acros, 99.5%), tetrahydrofuran (THF, Tedia), hexane (Acros), and *N*,*N*-dimethylformamide (DMF, Echo, 99.5%) were used as received. The diblock copolymer PCL-*b*-PEO-NH_2 and L-tyrosine *N*-carboxyanhydride (Tyr-NCA) was synthesized using previously reported procedures.[32–34,41,42]

Butyl-terminated poly-L-tyrosine (PTyr)

A solution of Tyr-NCA (5.64 g) in anhydrous DMF (10 mL) was stirred for 30 min and then Butylamine (0.10 g) was added through an Ar-purged syringe. After stirring for 24 h at 0 °C, the PTyr homopolymer was precipitated in cold ether and dried under vacuum at 50 °C (yield: 80%).

PCL-*b*-PEO-*b*-PTyr triblock copolymer

Tyr-NCA (1.12 g) and the macro-initiator PCL-*b*-PEO-NH_2 (0.70 g) were placed in a three-neck bottle, connected to a vacuum line, and then anhydrous DMF was added through a syringe. After stirring the solution for 24 h at 0 °C, the resulting copolymer was precipitated in cold methanol. The precipitate was re-dissolved in DMF, and then purified more than three times from methanol/ether to provide a solid powder that was dried under vacuum at 50 °C overnight (yield: 75%).

PTyrBZ and PCL-*b*-PEO-*b*-PTyrBZ triblock copolymer

A solution of aniline (1.54 g) and paraformaldehyde (0.99 g) in DMF was stirred for 1 h at 0 °C and then a solution of PTyr (2 g) or PCL-*b*-PEO-*b*-PTyr (0.24 g) in DMF was added *via* syringe. After stirring for 24 h under reflux at 75 °C, the polymer was precipitated in cold CH_3OH and then dried under

vacuum at 50 °C overnight (PTyrBZ: 80% yield; PCL-*b*-PEO-*b*-PTyrBZ: 85% yield).

Porous PTyrBZ structure

Desired amounts of PCL-*b*-PEO-*b*-PTyrBZ were placed on aluminum pans and polymerized using the following temperature profile: 150 °C for 2 h, 180 °C for 2 h, 210 °C for 2 h, 220 °C for 2 h, and 240 °C for 2 h. Upon increasing the curing temperature, the cured samples exhibited a red and dark appearance. After cooling the samples to 25 °C, pyrolysis of the cross-linked PCL-*b*-PEO-*b*-PTyrBZ was performed by heating very slowly (1 °C min^{-1}) from 25 to 330 °C and then maintaining the temperature at 330 °C for 2 h, without a protective gas atmosphere.

Characterization

Nuclear magnetic resonance (NMR) spectroscopy was performed using a Bruker 500 (500 MHz) spectrometer at room temperature, with a deuterated solvent as the internal standard and $CDCl_3$ as the solvent. Fourier transform infrared (FTIR) spectroscopy was performed using a Bruker Tensor 27 spectrophotometer, with 32 scans recorded at a spectral resolution of 4 cm^{-1}. Temperature-dependent FTIR spectra were recorded from the samples in a temperature-controlled compartment under a N_2 atmosphere to avoid thermal degradation during the measurement process. The thermal stabilities of the PCL-*b*-PEO diblock copolymer and the PTyrBZ homopolymer after curing under various conditions were measured under a N_2 atmosphere using a TA Q-50 TGA analyzer. The uncured and thermally cured PTyrBZ samples were placed in a Pt cell and heated from 30 to 800 °C under a N_2 atmosphere at a heating rate of 20 °C min^{-1}. The dynamic curing behavior and thermal transitions (T_g) of PTyr and PTyrBZ were measured under a N_2 atmosphere using a TA Q-20 DSC apparatus; the samples were placed in a sealed aluminum pan. The thermal dynamic curing behavior was identified during the first heating scan from room temperature to 250 °C at a heating rate of 10 °C min^{-1}; the values of T_g were determined from the second heating scan from room temperature to 250 °C at a heating rate of 10 °C min^{-1}. Small-angle X-ray scattering (SAXS) was performed at a wavelength (λ) of 1.24 Å at the BL17B3 beamline of the National Synchrotron Radiation Research Center (NSRRC), Taiwan. Wide-angle X-ray diffraction (WAXD) was performed using a wavelength of 1.32 Å at the BL17A1 wiggler beamline of the NSRRC. Transmission electron microscopy (TEM) was performed using a JEOL-JEM-2100 microscope operated at 200 kV. The porous samples obtained after thermal pyrolysis did not require staining because of the apparent difference in electron density between the block segment domains after selective degradation of PCL-*b*-PEO. The adsorption of MB was investigated using a UV–Vis–NIR spectrophotometer (Jasco, V-570), with deionized water as the solvent.

Results and discussion

Synthesis and thermal properties of PTyrBZ

Our objective in this study was to prepare a porous PTyr structure through selected thermal cancelation of the PCL-*b*-PEO block segments after thermal crosslinking of PCL-*b*-PEO-*b*-PTyrBZ. To examine the feasibility of presenting BZ units on the side chains of PTyr in PCL-*b*-PEO-*b*-PTyr, we first synthesized a BZ-functionalized PTyr homopolymer (PTyrBZ) as a model (Scheme 2). We prepared the model PTyrBZ through a

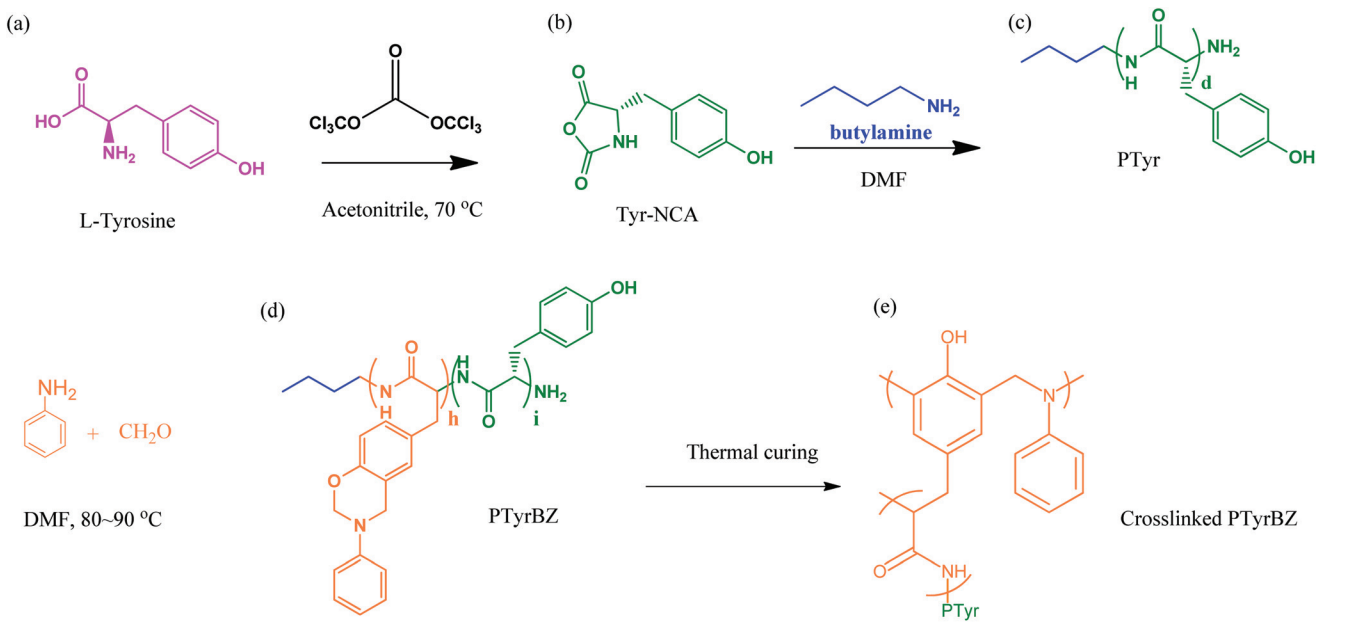

Scheme 2 Chemical structures and synthesis of (a) L-tyrosine, (b) the Tyr-NCA monomer, (c) the PTyr homopolymer, (d) the PTyrBZ random copolymer, and (e) the crosslinked PTyrBZ structure.

Mannich reaction of PTyr, CH_2O, and aniline in DMF at 75 °C for 24 h. Fig. S1† presents FTIR spectra, recorded at room temperature, of the Tyr-NCA monomer, the PTyr homopolymer, and the model PTyrBZ. In the spectrum of Tyr-NCA [Fig. S1(a)†], two characteristic C=O absorptions appear at 1765 and 1837 cm^{-1}, due to the C=O units b and a, respectively; signals for the aromatic ring appear at 1598 and 1609 cm^{-1}, and broad OH and sharp NH absorptions are located at 3100–3500 and 3307 cm^{-1}, respectively, confirming the formation of the Tyr-NCA ring. The spectrum recorded after ring opening polymerization of the Tyr-NCA monomer [Fig. S1(b)†], lacks the signals a and b of the C=O groups of the NCA ring, but features new absorptions at 1654 and 1631 (c) and 1540 (d) cm^{-1}, representing the amide I and amide II absorptions in the PTyr backbone; the broad OH and sharp NH absorptions remained at 3100–3500 cm^{-1}. The BZ structure of PTyrBZ was confirmed from its spectrum [Fig. S1(c)†] featuring new absorptions for oxazine rings at 933 cm^{-1} and for C–O–C stretching at 1238 cm^{-1}. Fig. 1 presents the corresponding ^1H NMR spectra of the Tyr monomer, the PTyr homopolymer, and the model PTyrBZ. The spectrum of the Tyr-NCA monomer [Fig. 1(a)] features a signal at 9.04 ppm representing the phenolic OH unit (peak m); the signal of the NH unit appeared at 9.34 ppm (peak h); the aromatic ring was represented by two doublets at 6.66 and 6.97 ppm (peaks l and k, respectively); and the alkyl CH (peak j) and CH_2 (peak i) protons were represented by a doublet at 2.49 ppm and a triplet at 4.66 ppm, respectively. After ROP, the spectrum of the PTyr homopolymer [Fig. 1(b)] featured signals for the phenolic OH group at 9.11 ppm, the NH unit at 7.95 ppm (singlet), the aromatic protons at 6.95 and 6.57 ppm, the methine (CH) proton at 4.40 ppm, and the CH_3 unit (peak q; a triplet arising from initiator, butylamine) at 0.81 ppm, with other peaks representing the CH_2 protons of butylamine as multiplets at 1.14, 1.26, and 2.63 ppm. We could use this ^1H NMR spectrum to calculate the molecular weight of PTyr from the peak intensity ratio of peaks q and i; we obtained a degree of polymerization for the PTyr homopolymer of 24. The signals of the BZ ring in the spectrum of PTyrBZ [Fig. 1(c)] appeared as two characteristic bands at 5.79 ppm (OCH_2N, peak v) and 4.85 ppm ($ArCH_2N$, peak u); the integration intensity ratio of these two bands was close to 1 : 1, indicating that the synthesis of PTyrBZ was successful. By calculating the peak ratio of the oxazine ring (peak u or v) of PTyrBZ and the phenolic OH unit (peak m) of PTyr, we obtained a BZ ring concentration in PTyrBZ of 56%; this value is close to that (64%) reported previously when using poly(vinyl phenol) (PVPh) to prepare BZ-functionalized PVPh.[43] Taken together, these FTIR and NMR spectral data confirmed the successful synthesis of PTyrBZ.

To investigate the thermal curing behavior and thermal properties of PTyrBZ, we first used DSC and FTIR spectroscopic analyses to study the thermal ROP of PTyrBZ. Fig. 2(a) presents the DSC thermogram of PTyrBZ recorded under a N_2 atmosphere; it displays a maximum exothermic peak at 223 °C and a heat of polymerization of 59.0 J g^{-1}. Compared with the model Pa-type of BZ monomer, prepared from phenol, CH_2O, and aniline,[35] the curing temperature of PTyrBZ had shifted from 263 °C (for Pa) to 223 °C, indicating that the phenolic OH groups and the amide groups of the backbone could function as basic catalysts that contributed to lowering the temperature of thermal polymerization.[35,44,45] Fig. 3 presents the corresponding FTIR spectra of PTyrBZ recorded after curing

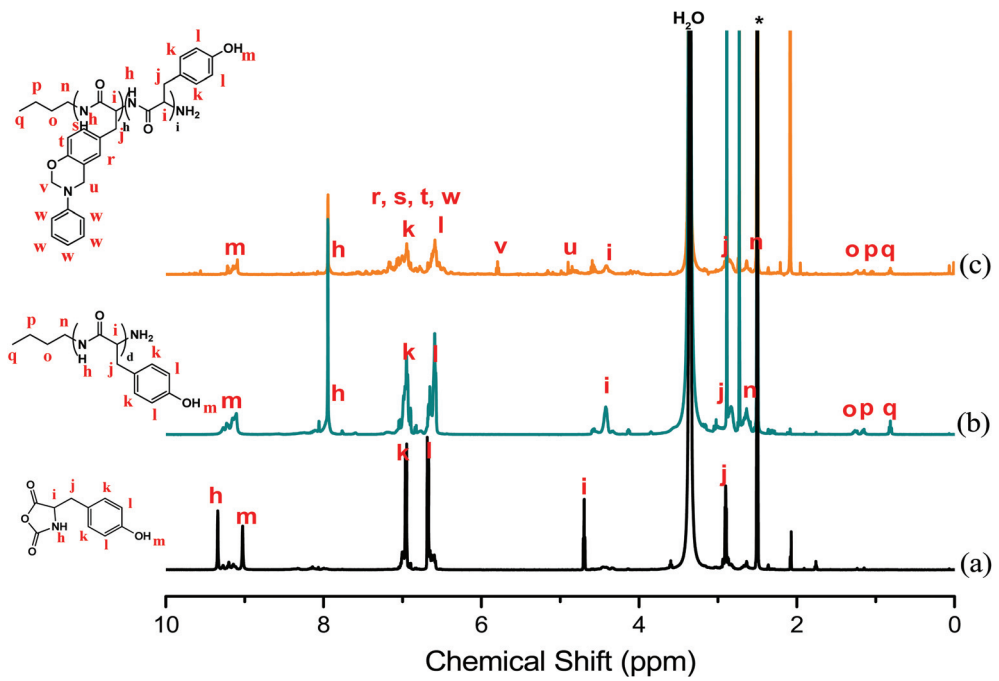

Fig. 1 ^1H NMR spectra of (a) the Tyr-NCA monomer, (b) the PTyr homopolymer, and (c) the PTyrBZ random copolymer.

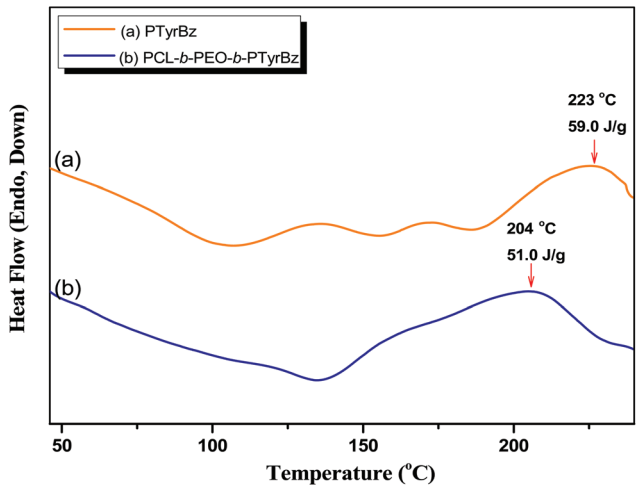

Fig. 2 DSC thermograms (first heating scans) of (a) PTyrBZ and (b) PCL-*b*-PEO-*b*-PTyrBZ.

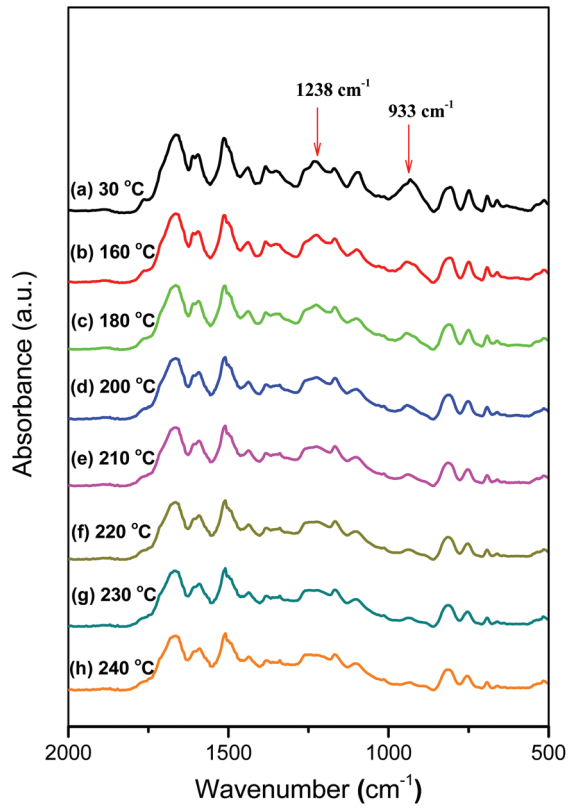

Fig. 3 FTIR spectra of PTyrBZ recorded after each heating stage.

under various conditions. The intensity of the signal for the BZ ring at 933 cm^{-1} decreased upon increasing the curing temperature and almost disappeared when the curing temperature was 240 °C, implying that thermal ROP had occurred. Furthermore, the glass transition temperature of PTyrBZ after thermal curing at 240 °C was 209 °C [Fig. 4(b)]; this value is significantly higher than that of pure PTyr (*i.e.*, without BZ

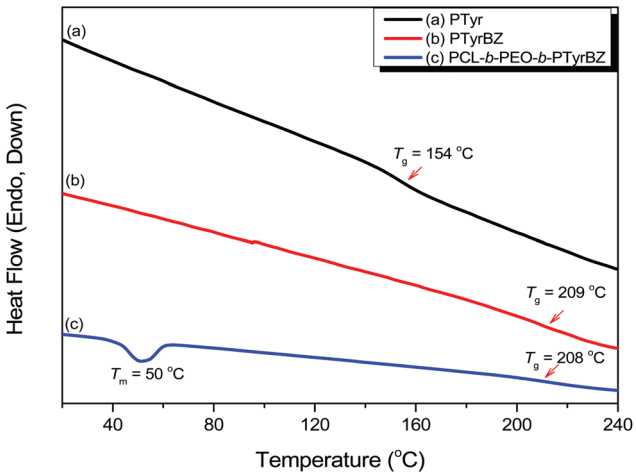

Fig. 4 DSC thermograms (second heating scans) of (a) PTyr, (b) PTyrBZ, and (c) PCL-*b*-PEO-*b*-PTyrBZ after thermal polymerization.

units) [T_g = 154 °C; Fig. 4(a)],[32] as measured using DSC. These findings suggested that the BZ units could indeed be forming 3D network structures that restricted the molecular motion of PTyrBZ and, as a result, increase its value of T_g.

Synthesis and thermal properties of PCL-*b*-PEO-*b*-PTyrBZ

Fig. 5 displays the ambient-temperature FTIR spectra of the PCL-*b*-PEO-NH_2 diblock copolymer, the Tyr-NCA monomer, and the triblock copolymers PCL-*b*-PEO-*b*-PTyr and PCL-*b*-PEO-*b*-PTyrBZ. The spectrum of the PCL-*b*-PEO-NH_2 diblock copolymer [Fig. 5(a)] features two signals for C=O stretching at 1734 and 1724 cm^{-1} of the PCL segment, representing amorphous and crystalline domains, respectively; the PEO block segment provided a characteristic peak at 1106 cm^{-1} for ether stretching. Similar to that of pure PTyr, the spectrum of the PCL-*b*-PEO-*b*-PTyr triblock copolymer, presented in Fig. 5(c), exhibits new signals at 1658 (peak e) and 1541 (peak f) cm^{-1}, corresponding to the amide I and amide II absorptions of the PTyr segment. The BZ units of PCL-*b*-PEO-*b*-PTyrBZ were evident in its spectrum [Fig. 5(d)] as a signal at 947 cm^{-1}, representing the oxazine ring.

Fig. 6 presents the corresponding ^{1}H NMR spectra of the PCL-*b*-PEO-NH_2 diblock copolymer, the Tyr-NCA monomer, and the triblock copolymers PCL-*b*-PEO-*b*-PTyr and PCL-*b*-PEO-*b*-PTyrBZ. The spectrum of the PCL-*b*-PEO diblock copolymer features [Fig. 6(a)] signals for the methylene unit (OCH_2) of the PCL segment at 4.10 ppm (peak g) and for the ethylene unit (CH_2OCH_2) of the PEO block segment at 3.65 ppm (peak a). The spectrum of the PCL-*b*-PEO-*b*-PTyr triblock copolymer [Fig. 6(c)] features the following signals of the PTyr block segment: for the NH units at 7.95 ppm (singlet), the phenolic OH groups at 9.11 ppm, the aromatic protons at 6.95 and 6.57 ppm, and the methine (CH) protons at 4.40 ppm. Again, we could calculate the molecular weight of the PTyr block segment from this ^{1}H NMR spectrum by measuring the peak intensity ratio of peaks g and i; we obtained a degree of

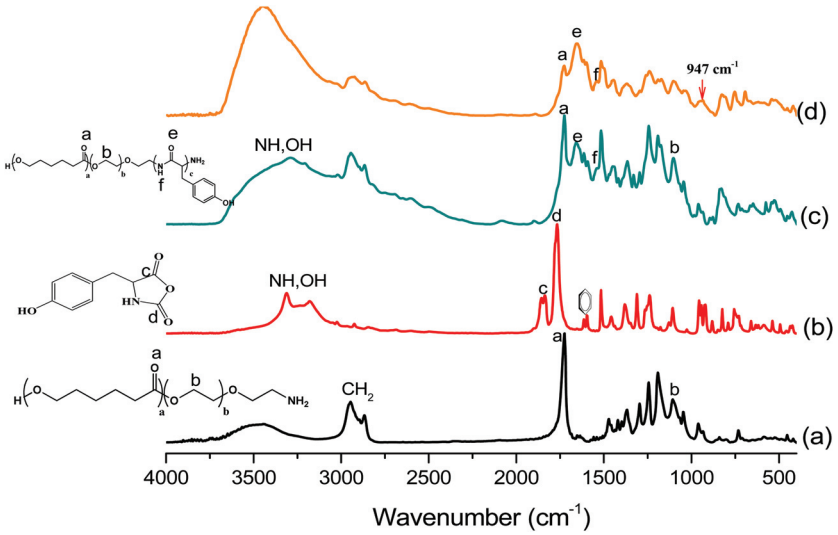

Fig. 5 FTIR spectra of (a) PCL_{88}-*b*-PEO_{68}-NH_2, (b) the Tyr-NCA monomer, (c) PCL_{88}-*b*-PEO_{68}-*b*-$PTyr_{24}$, and (d) PCL-*b*-PEO-*b*-PTyrBZ.

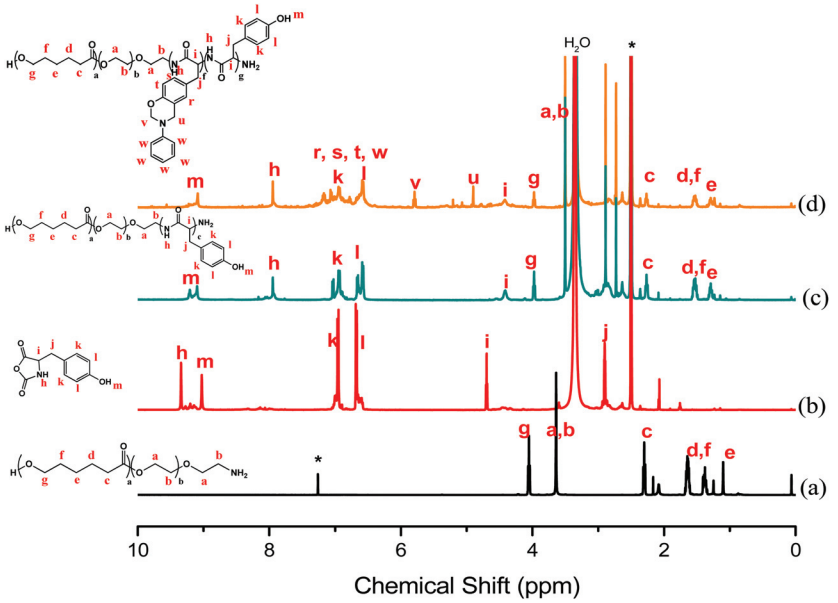

Fig. 6 ^{1}H NMR spectra of (a) PCL_{88}-*b*-PEO_{68}-NH_2, (b) the Tyr-NCA monomer, (c) PCL_{88}-*b*-PEO_{68}-*b*-$PTyr_{84}$, and (d) PCL-*b*-PEO-*b*-PTyrBZ.

polymerization for the PTyr block segment of 84. Furthermore, GPC analysis of the PCL-*b*-PEO-*b*-PTyr triblock copolymer suggested (Fig. S2†) narrow polydispersity, with a shift of the signal to a lower retention time relative to that of pure PCL-*b*-PEO, again suggesting the successful synthesis of PCL-*b*-PEO-*b*-PTyr. Fig. 6(d) presents the ^{1}H NMR spectrum of the PCL-*b*-PEO-*b*-PTyrBZ triblock copolymer; the presence of the BZ rings was evident from the presence of two characteristic bands at 5.79 ppm (OCH_2N, peak v) and 4.89 ppm ($ArCH_2N$, peak u); the integration intensity ratio of these two bands was close to 1 : 1, as would be expected for the successful synthesis of the PCL-*b*-PEO-*b*-PTyrBZ triblock copolymer. By calculating the peak area ratio of the signals for the oxazine rings (peak u or v) of the PTyrBZ block segment and the phenolic OH groups (peak m) of the PTyr block segment, we determined that the BZ ring concentration in the PTyrBZ block segment was 74%. Thus, these FTIR and NMR spectral analyses confirmed the successful synthesis of the PCL-*b*-PEO-*b*-PTyrBZ triblock copolymer.

Again, we used DSC and FTIR spectroscopic analyses to investigate the thermal ROP of PCL-*b*-PEO-*b*-PTyrBZ. Fig. 2(b) presents the DSC thermogram of PCL-*b*-PEO-*b*-PTyrBZ, recorded under a N_2 atmosphere; a maximum exothermic peak appeared at 204 °C, and the heat of polymerization was 51.0 J g^{-1}. These values suggest that the residual phenolic OH groups and the amide groups of the backbone also could act

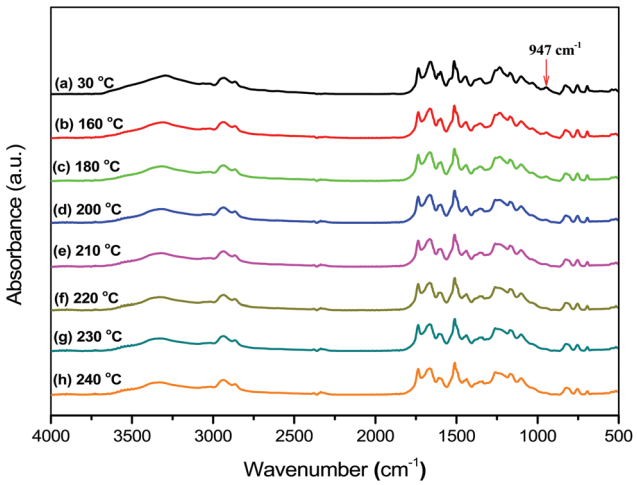

Fig. 7 FTIR spectra of the PCL-*b*-PEO-*b*-PTyrBZ triblock copolymer after each heating stage.

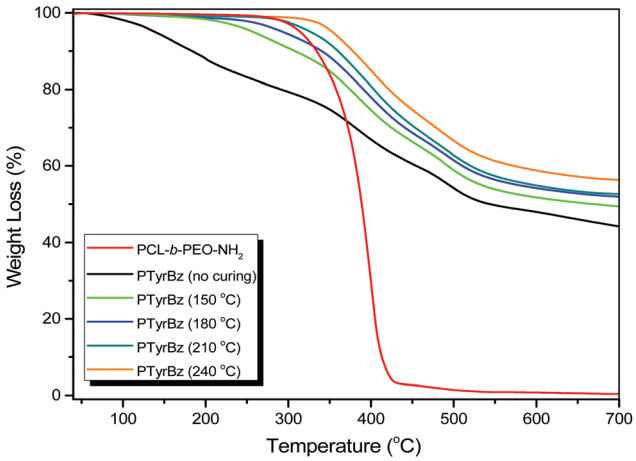

Fig. 8 TGA analyses of PCL-*b*-PEO and PTyrBZ after each heating stage.

as basic catalysts that contributed to the thermal polymerization occurring at a lower temperature. In addition, the lower glass transition temperatures of the PCL and PEO block segments presumably improved the mobility of PCL-*b*-PEO-*b*-PTyrBZ, thereby lowering the thermal curing temperature of the PTyrBZ block segment (204 °C) relative to that of the pure PTyrBZ homopolymer (223 °C). Fig. 7 displays the FTIR spectra of PCL-*b*-PEO-*b*-PTyrBZ recorded after curing at various temperatures. The intensity of the signal for the BZ ring at 947 cm^{-1} decreased upon increasing the curing temperature, almost disappearing when the curing temperature was 220 °C; this value is lower than that of the pure PTyrBZ homopolymer. In addition, the glass transition temperature of the PTyrBZ block segment in the PCL-*b*-PEO-*b*-PTyrBZ triblock copolymer after thermal curing at 240 °C remained at 208 °C [Fig. 4(c)] when compared with pure PTyrBZ after thermal curing. In addition, we observed a melting peak at approximately 50 °C that probably corresponds to melting of the PCL or PEO block segment, suggesting that microphase separation of the PCL or PEO block segment may have occurred after thermal curing of the PTyrBZ block segment, due to so-called "reaction-induced microphase separation" [Scheme 1(d)].[23]

Functionalized porous PTyr structure

To ensure the successful preparation of a functionalized porous PTyr structure, we examined the thermal stability of the pure PCL-*b*-PEO diblock copolymer and the pure PTyrBZ homopolymer after curing at various temperatures under a N_2 atmosphere (Fig. 8). The thermal degradation temperature [10% weight loss temperature (T_{d10})] of the pure PCL-*b*-PEO diblock copolymer was 330 °C; it displayed 94 wt% loss under air [19]. For the pure PTyrBZ homopolymer, the char yield and the values of T_{d10} both increased upon increasing the curing temperature. The uncured PTyrBZ exhibited only a single value of T_{d10} at 183 °C and a char yield of 41.1%; both values are significantly lower than those of the pure PCL-*b*-PEO diblock copolymer. Nevertheless, these values increased to 380 °C and 60%, respectively, after the thermal curing of PTyrBZ at 240 °C; this value of T_d is already higher than that of the PCL-*b*-PEO diblock copolymer. Thus, the incorporation of BZ units on the side chains of PTyr not only improved the glass transition temperature but also the thermal degradation behavior after thermal curing.

As a result, we examined the pyrolysis of the thermally cured PCL-*b*-PEO-*b*-PTyrBZ sample at temperatures from 25 to 330 °C, without the protective gas atmosphere, at a heating rate of 1 °C min^{-1}. The selective removal of the PCL-*b*-PEO block segment was first confirmed through FTIR spectral analyses (Fig. S3†). The signal for the BZ ring at 947 cm^{-1} was absent, but those for the C=O unit of the PCL clock, C–O–C unit of the PEO block, and the amide I absorption remained, after thermal curing of PCL-*b*-PEO-*b*-PTyrBZ at 240 °C. The intensities of the signals for the C=O groups of the PCL block and the C–O–C units of the PEO block both decreased significantly after thermal calcination at 330 °C, but the amide I absorption remained for the PTyr segment. To confirm the disappearance of the PCL-*b*-PEO block segment of the porous PTyr structure, we took advantage of the intrinsic crystallization behavior of PCL and PEO block segments and recorded WAXD and SAXS patterns.

Fig. 9 presents the WAXD analyses of (a) PCL-*b*-PEO-NH_2, (b) PCL-*b*-PEO-*b*-PTyr, (c) PCL-*b*-PEO-*b*-PTyrBZ, (d) PCL-*b*-PEO-*b*-PTyrBZ (after thermal curing at 240 °C), and (e) PCL-*b*-PEO-*b*-PTyrBZ (after thermal calcination at 330 °C), recorded at room temperature (Fig. 9(A)) and at 120 °C (Fig. 9(B)). Two strong $(200)_{PCL}$ and $(110)_{PCL}$ diffraction peaks appear in Fig. 9(A)-(a), but the $(120)_{PEO}$ diffraction peak was not evident because of the confinement effect for the PCL-*b*-PEO-NH_2 diblock copolymer.[46] The crystallization peaks from the PCL segment disappeared completely when the temperature (120 °C) was higher than the melting temperature (75 °C) of PCL, as displayed in Fig. 9(B). Furthermore, these two crystallization

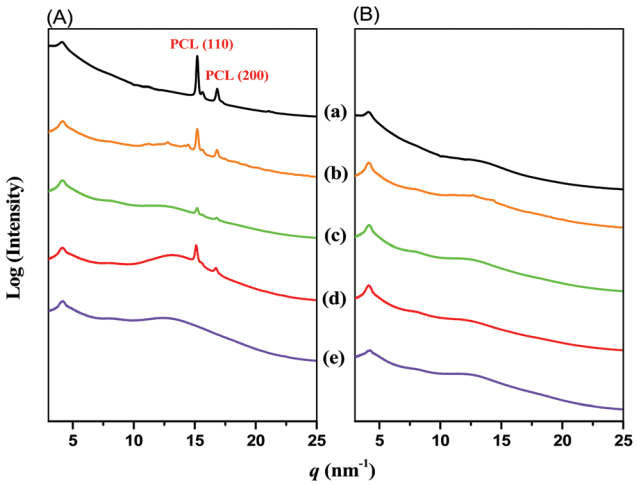

Fig. 9 WAXD patterns, recorded at (A) room temperature and (B) 120 °C, of (a) PCL-*b*-PEO-NH_2, (b) PCL-*b*-PEO-*b*-PTyr, (c) PCL-*b*-PEO-*b*-PTyrBZ, (d) PCL-*b*-PEO-*b*-PTyrBZ after thermal curing at 240 °C, and (e) PCL-*b*-PEO-*b*-PTyrBZ after thermal calcination at 330 °C to form the porous PTyr.

peaks remained in the patterns for PCL-*b*-PEO-*b*-PTyr, PCL-*b*-PEO-*b*-PTyrBZ, and even PCL-*b*-PEO-*b*-PTyrBZ after thermal curing at 240 °C, implying that the PCL segment underwent microphase separation in these triblock copolymer systems. In contrast, the crystallization peaks of the thermally cured PCL-*b*-PEO-*b*-PTyrBZ disappeared completely after thermal calcination at 330 °C, indicating that porous PTyr may have formed after this procedure.

Fig. S4† displays corresponding SAXS analyses of (a) PCL-*b*-PEO-NH_2, (b) PCL-*b*-PEO-*b*-PTyr, (c) PCL-*b*-PEO-*b*-PTyrBZ, (d) PCL-*b*-PEO-*b*-PTyrBZ (after thermal curing at 240 °C), and (e) PCL-*b*-PEO-*b*-PTyrBZ (after thermal calcination at 330 °C), recorded at room temperature. The pattern of pure PCL-*b*-PEO-NH_2 [Fig. 10(a)] features a peak ratio of 1 : 3; the first peak was located at a value of q^* of 0.44 nm^{-1} (d = 14.27 nm) because of crystallization-induced microphase separation of the PCL segment.[46] After ROP polymerization of PCL-*b*-PEO-*b*-PTyr, the SAXS pattern displays only the broad peak at a value of q^* of 0.32 nm^{-1} (d = 19.62 nm). Furthermore, disordered structures with no obvious peaks were observed in the SAXS patterns of PCL-*b*-PEO-*b*-PTyrBZ, PCL-*b*-PEO-*b*-PTyrBZ after thermal curing at 240 °C, and PCL-*b*-PEO-*b*-PTyrBZ after thermal calcination at 330 °C. The porous PTyr structure was confirmed through TEM analyses (Fig. 10). No obvious structure was observed for PCL-*b*-PEO-*b*-PTyrBZ after thermal curing at 240 °C [Fig. 10(a) and (b)], but a structure with pore diameters of 15–20 nm was evident for PCL-*b*-PEO-*b*-PTyrBZ after thermal calcination at 330 °C [Fig. 10(c) and (d)]. Such a porous PTyr structure with functional phenolic OH groups and amide groups would be expected after thermal calcination. We used an aqueous solution of MB (10^{-4} wt%, 6 mL) to investigate the adsorption equilibrium of the porous PTyr structure

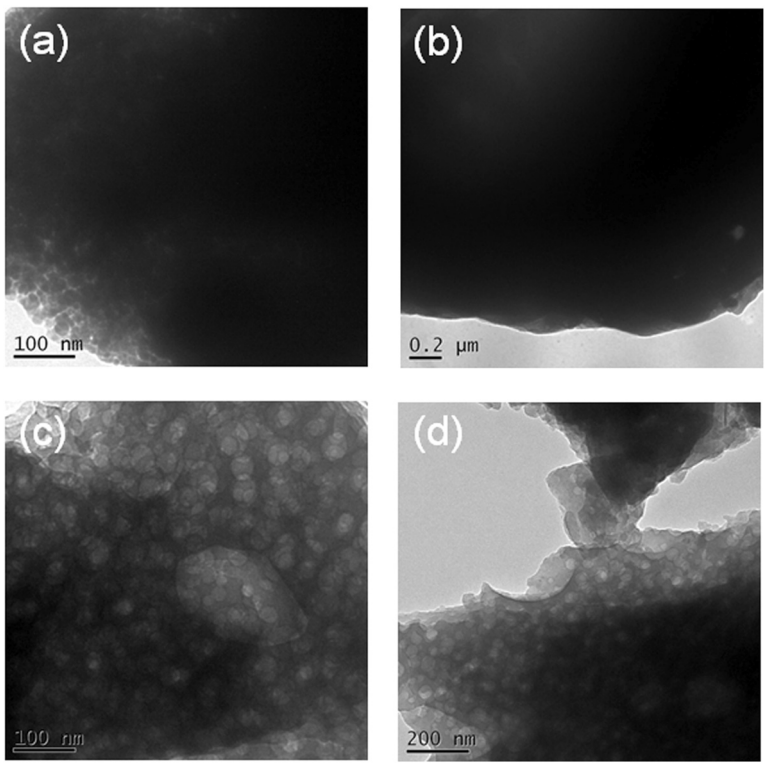

Fig. 10 TEM images of (a, b) PCL-*b*-PEO-*b*-PTyrBZ after thermal curing at 240 °C and (c, d) PCL-*b*-PEO-*b*-PTyrBZ after thermal calcination at 330 °C to form the functional porous PTyr.

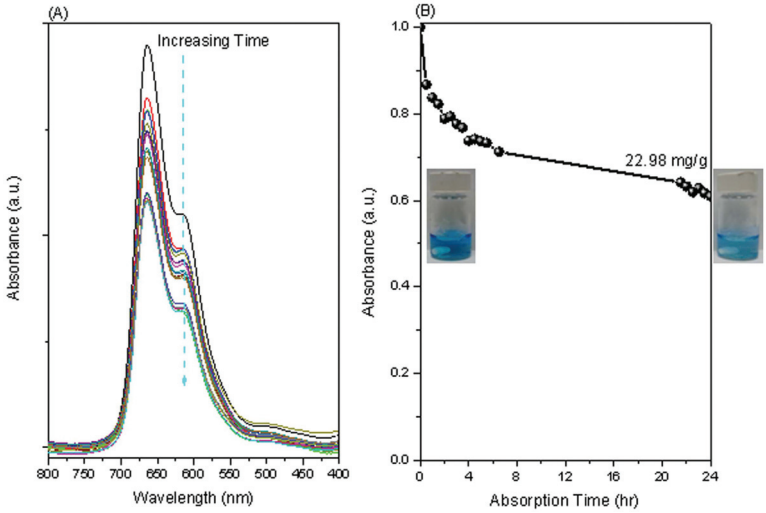

Fig. 11 (A) UV–Vis spectra of the functional porous PTyr recorded at various MB adsorption times. (B) Absorbance ratios of MB plotted over 24 h.

(0.01 g) at room temperature. Fig. 11 displays the resulting UV–Vis absorption spectra; the intensity of the signals at 615 and 665 nm decreased upon increasing the absorption time. The mass balance relationship could be calculated using the equation:

$$q_e(C_0 - C_e)V/W,$$

where V is the solution volume (mL); C_e and C_0 are the equilibrium and initial MB concentrations (mg mL^{-1}), respectively; and W is the weight of the porous PTyr (g). The final value of q_e, determined from the mass balance relationship, was 22.98 mg g^{-1} for the porous PTyr; this value is significantly higher than that we obtained previously[16] for the mesoporous silica incorporating PTyr (4.537 mg g^{-1}) and that of another system from another research group.[47] Furthermore, we suspect that such a bio-based porous PTyr might also find use in drug delivery; for example, for the delivery of procainamide hydrochloride and doxorubicin (DOX).[48–50]

Conclusions

We have synthesized a new PCL-*b*-PEO-*b*-PTyr triblock copolymer through sequential ROP; we confirmed its structure through FTIR and NMR spectral analyses. The incorporation of BZ units into PCL-*b*-PEO-*b*-PTyr resulted in the formation of a PCL-*b*-PEO-*b*-PTyrBZ triblock copolymer that could form a 3D network structure after thermal polymerization of its BZ units, thereby increasing the thermal stability of the PTyr segment and allowing selective thermal cancelation of the PCL-*b*-PEO block segment. After performing those procedures, the functional porous PTyr structure featuring phenolic OH and amide groups could hydrogen bonding with MB, resulting in dye adsorption that was more highly efficient than that obtained with other biomaterial-related compounds.

Conflicts of interest

There are no conflicts to declare.

Acknowledgements

This study was supported financially by the Ministry of Science and Technology, Taiwan, under contracts MOST 106-2221-E-110-067-MY3 and 105-2221-E-110-092-MY3. This work also supported by the National Natural Science Foundation of China (51773214).

References

1 J. Deming, *Chem. Rev.*, 2016, **116**, 786–808.
2 H. Lu, J. Wang, Z. Song, L. Yin, Y. Zhang, H. Tang, C. Tu, Y. Lin and J. Cheng, *Chem. Commun.*, 2014, **50**, 139–155.
3 J. Zhang, C. Gong, B. Q. Li, M. Shan and G. L. Wu, *J. Polym. Res.*, 2017, **24**, 122.
4 K. Bauri, M. Nandi and P. De, *Polym. Chem.*, 2018, **9**, 1257–1287.
5 S. Guragain, B. P. Bastakoti, V. Malgras, K. Nakashima and Y. Yamauch, *Chem. – Eur. J.*, 2015, **21**, 13164–13174.
6 C. Hua, C. M. Dong and Y. Wei, *Biomacromolecules*, 2009, **10**, 1140–1148.
7 V. K. Kotharangannagari, A. Sanchez-Ferrer, J. Ruokolainen and R. Mezzenga, *Macromolecules*, 2011, **44**, 4569–4573.
8 P. C. Li, Y. C. Lin, M. Chen and S. W. Kuo, *Soft Matter*, 2013, **9**, 11257–11269.
9 Y. C. Lin and S. W. Kuo, *Polym. Chem.*, 2012, **3**, 882–891.
10 C. Bonduelle, *Polym. Chem.*, 2018, **9**, 1517–1529.
11 H. A. Klok, J. F. Langenwalter and S. Lecommandoux, *Macromolecules*, 2000, **33**, 7819–7826.

12 P. Papadopoulos, G. Floudas, H. A. Klok, I. Schnell and T. Pakula, *Biomacromolecules*, 2004, **5**, 81–91.
13 C. Cai, J. Lin, Y. Lu, Q. Zhang and L. Wang, *Chem. Soc. Rev.*, 2016, **45**, 5985–6012.
14 S. W. Kuo, H. F. Lee, C. F. Huang, C. F. Huang and F. C. Chang, *J. Polym. Sci., Part A: Polym. Chem.*, 2008, **46**, 3108–3119.
15 S. W. Kuo, H. F. Lee, W. J. Huang, K. U. Jeong and F. C. Chang, *Macromolecules*, 2009, **42**, 1619–1626.
16 Y. S. Lu, B. P. Bastakoti, M. Pramanik, Y. Yamauchi and S. W. Kuo, *Chem. – Eur. J.*, 2016, **22**, 1159–1164.
17 J. Fang, Q. Yong, K. Zhang, W. Sun, S. Yan, L. Cui and J. Yin, *J. Mater. Chem. B*, 2015, **3**, 1020–1031.
18 B. Cao, J. Yin, S. Yan, L. Cui, X. Chen and Y. Xie, *Macromol. Biosci.*, 2011, **11**, 427–434.
19 J. G. Li, Y. D. Lin and S. W. Kuo, *Macromolecules*, 2011, **44**, 9295–9309.
20 J. G. Li, C. Y. Chuang and S. W. Kuo, *J. Mater. Chem.*, 2012, **22**, 18583–18595.
21 W. C. Chu, J. G. Li and S. W. Kuo, *RSC Adv.*, 2013, **3**, 6485–6498.
22 W. C. Chu, B. P. Bastakoti, Y. V. Kaneti, J. G. Li, Y. Yamauchi, H. R. Alamri, Z. A. Alothman and S. W. Kuo, *Chem. – Eur. J.*, 2017, **23**, 13734–13741.
23 D. Hu, Z. Xu, K. Zeng and S. Zheng, *Macromolecules*, 2010, **43**, 2960–2969.
24 Y. Deng, T. Yu, Y. Wang, Y. Shi, Y. Meng, D. Gu, L. Zhang, Y. Huang, C. Liu, X. Wu and D. Zhao, *J. Am. Chem. Soc.*, 2007, **29**, 1690–1697.
25 S. Valkama, A. Nykanen, H. Kosonen, R. Ramani, F. Tuomisto, P. Engelhardt, G. ten-Brinke, O. Ikkala and J. Ruokolainen, *Adv. Funct. Mater.*, 2007, **17**, 183–190.
26 H. Kosenen, S. Valkama, A. Nykanen, M. Toivanen, G. ten-Brinke, J. Ruokolainen and O. Ikkala, *Adv. Mater.*, 2006, **18**, 201–205.
27 W. C. Chu, J. G. Li, C. F. Wang, K. U. Jeong and S. W. Kuo, *J. Polym. Res.*, 2013, **20**, 272.
28 R. Dawson, A. I. Cooper and D. J. Adams, *Prog. Polym. Sci.*, 2012, **37**, 530–563.
29 J. G. Li, T. S. Lee, K. U. Jeong, C. H. Lin and S. W. Kuo, *RSC Adv.*, 2012, **2**, 11242–11244.
30 W. C. Chu, D. R. Peng, B. P. Bastakoti, M. Parmanik, V. Malgras, T. Ahamad, S. M. Alshehri, Y. Yamauchi and S. W. Kuo, *ChemistrySelect*, 2016, **1**, 1339–1346.
31 Y. S. Lu and S. W. Kuo, *RSC Adv.*, 2015, **5**, 88539–88547.
32 Y. S. Lu, Y. C. Lin and S. W. Kuo, *Macromolecules*, 2012, **45**, 6547–6556.
33 M. G. Mohamed, F. H. Lu, J. L. Hong and S. W. Kuo, *Polym. Chem.*, 2015, **6**, 6340–6350.
34 Y. R. Jheng, M. G. Mohamed and S. W. Kuo, *Polymers*, 2017, **9**, 503.
35 H. Ishida, *Overview and historical background of polybenzoxazine research in Handbook of Benzoxazine Resins*, Elsevier, Amsterdam, 2011, pp. 1–84.
36 C. F. Wang, Y. C. Su, S. W. Kuo, C. F. Huang, Y. C. Sheen and F. C. Chang, *Angew. Chem., Int. Ed.*, 2006, **45**, 2248–2251.
37 T. Zhang, H. Yan, Z. Fang, E. Yuping, T. Wu and F. Chen, *Appl. Surf. Sci.*, 2014, **309**, 218–224.
38 J. Y. Wu, M. G. Mohamed and S. W. Kuo, *Polym. Chem.*, 2017, **8**, 5481–5489.
39 A. F. M. El-Mahdy and S. W. Kuo, *Polym. Chem.*, 2018, **9**, 1815–1826.
40 H. K. Shih, Y. L. Chu, F. C. Chang, C. Y. Zhu and S. W. Kuo, *Polym. Chem.*, 2015, **6**, 6227–6237.
41 Y. Wan, Z. Gan and Z. Li, *Polym. Chem.*, 2014, **5**, 1720–1727.
42 C. C. Tsai, Z. Gan, T. Chen and S. W. Kuo, *Macromolecules*, 2108, **51**, 3017–3029.
43 H. Kimura, A. Matsumoto, H. Sugito, K. Hasegawa, K. Ohtsuka and A. Fukuda, *J. Appl. Polym. Sci.*, 2001, **79**, 555–565.
44 M. G. Mohamed, R. C. Lin, J. H. Tu, J. L. Hong and S. W. Kuo, *RSC Adv.*, 2015, **5**, 65635–65645.
45 M. G. Mohamed, C. H. Hsiao, F. Luo, L. Dai and S. W. Kuo, *RSC Adv.*, 2015, **5**, 45201–45212.
46 Y. W. Chiang, Y. Y. Hu, J. N. Li, S. H. Huang and S. W. Kuo, *Macromolecules*, 2015, **48**, 8526–8533.
47 G. Annadurai, R. S. Juang and D. J. Lee, *J. Hazard. Mater.*, 2002, **92**, 263–274.
48 W. C. Chu, C. C. Cheng, B. P. Bastakoti and S. W. Kuo, *RSC Adv.*, 2016, **6**, 33811–33820.
49 G. H. Van Domeselaar, G. S. Kwon, L. C. Andrew and D. S. Wishart, *Colloids Surf., B*, 2003, **30**, 323–334.
50 P. Markland, G. L. Amidon and V. C. Yang, *Int. J. Pharm.*, 1999, **178**, 183–192.